INTERNATIONAL JOURNAL OF AUTOMOTIVE AND MECHANICAL ENGINEERING
ISSN: 2229-8649 e-ISSN: 2180-1606
VOLUME 23, ISSUE 2, 2026, 13516 - 13527
DOI: https://doi.org/10.15282/ijame.23.2.2026.4.1023

RESEARCH ARTICLE

Optimization of bus seat vibration isolation by experiment and metaheuristic approaches

Zamri Mohamed[1]*, S.M. Tasnim Mahbub[1], Rozieana Khairuddin[2]

[1]Faculty of Mechanical & Automotive Engineering Technology, Universiti Malaysia Pahang Al-Sultan Abdullah, 26000 Pekan, Pahang, Malaysia
[2]Center for Mathematical Sciences, Universiti Malaysia Pahang Al-Sultan Abdullah, 26000 Pekan, Pahang, Malaysia

Abstract - One way of determining health risk to public transport passengers is by measuring whole-body vibration (WBV) according to ISO 2631-1 standard. This Standard specifies the measurement and evaluation of RMS acceleration and Vibration Dose Value (VDV) in the range 0.5–80 Hz along three axes, using specific frequency-weighting curves. On longer routes over rough road surfaces, this measurement will help assess short- and long-term health effects. Existing bus seats are commonly bolted to the floor without vibration isolation, which may amplify vibration transmitted to passengers. This study aims to characterize and optimize the use of a passive rubber damper by integrating an EMT-FEA-PSO framework into an unmodified twin-seat passenger bus structure. Experimental Modal Testing (EMT) identified six dominant vibration modes in the 20–100 Hz range, which are validated against a Finite Element Analysis (FEA) model with an error within 10–15%. On-road measurements revealed that SEAT values consistently above 100% at speeds of 30–80 km/h, confirming vibration amplification by the unmodified seat. In laboratory tests, three rubber isolators were evaluated for effectiveness, and one damper reduced RMS acceleration by approximately 33%. Next, Particle Swarm Optimization (PSO) was applied to a 2-DOF seat–floor model to determine optimal damper stiffness, where the PSO-simulated FRF shows clear resonance peak attenuation. The proposed methodology offers a practical, low-cost design guidance tool for improving WBV isolation in bus seating and can be extended to other vehicle or machinery support structures.

Article History
Received : 15 October 2025
Revised : 5 May 2026
Accepted : 15 May 2026
Published : 30 June 2026

Keywords
Bus seat vibration
Vibration mitigation
Vibration optimization

1. Introduction

Prior research has extensively documented that whole-body vibration (WBV) across various transportation modes, including helicopters, transit buses, and passenger vehicles, induces significant subjective discomfort and motion sickness among occupants [1-4]. Furthermore, prolonged exposure to these vibrational environments has been strongly linked to adverse physiological and biomechanical outcomes, including elevated heart rate, accelerated musculoskeletal disorders, changes in bone mineral density, and severe low-back or intervertebral disc strain [5-9]. Whole-body vibration (WBV) is defined as vibrations experienced by the human body, which can contribute to discomfort, fatigue, and long-term musculoskeletal risks [10-13]. Passenger comfort and safety on longer trips over rough roads are important concerns. The transmission of vibration amplitude through the bus chassis and directly to the passenger seats without isolation may significantly affect passenger health outcomes [14-15]. According to [16], a study conducted in Malaysia found that WBV exposure may cause fatigue and back discomfort. The sources of discomfort and fatigue are usually transmitted vibration from tire-road interaction, rather than engine- or wind-induced vibration. Having a WBV standard to determine discomfort level will enable categorization of vibration amplitude to be compared with other studies.

The two standards commonly used to compare vibration amplitude and discomfort level are British Standard BS 6841 (1987) and International Standard ISO 2631 (1997) [17]. The Seat Effective Amplitude Transmissibility (SEAT) criterion specifies the effectiveness of seat vibration isolation. Measuring SEAT values at the seat base and the floor enables calculation of transmissibility, the ratio of vibration transmitted to the passenger's seat from the floor. Prior studies have used SEAT to assess dynamic comfort in vehicles [18], establish relationships between vibration transmissibility and human perception [19], and evaluate health risks in transportation contexts [20]. Other studies also included a biomechanical vibration model to represent the coupled interaction between the seat and the seated human body, which was stated to improve vertical transmissibility prediction accuracy [21].

Passive vibration isolation technique using rubber mounts is commonly implemented at support interfaces to reduce vibration transmission for machinery support structures. In the same way, we aim to apply the same technique to investigate the potential for reducing vibration in passenger bus seats. To investigate vibration reduction, Experimental Modal Testing (EMT) and Finite Element Analysis (FEA) are employed to characterize the dynamic properties of seating systems, including mode shapes and natural frequencies. In another study, both methods are used to verify each other before the results are used to support the parametric and transmissibility study [22-23]. In that study, vibration transmissibility depended on the isolators' stiffness and damping characteristics, suggesting that properly tuned isolators can significantly reduce vibration. Similarly, a poorly tuned isolator may amplify vibration [24]. In short, a systematic evaluation of damper parameters is essential to ensure effective vibration control for machinery structures and human support structures.

***CORRESPONDING AUTHOR | Zamri Mohamed** | ✉ zamrim@umpsa.edu.my

Various methods have been implemented to optimize the ground vehicle vibration problem [25-27]. These include computer algorithms, active hardware implementation, and passive vibration control [28-30]. Metaheuristic algorithms, such as Particle Swarm Optimization (PSO), mimic natural phenomena to find the maximum or minimum of an objective function while satisfying specific constraints. Natural processes often inspire these optimization techniques to solve various problems, including those in engineering and vibration topics. There are other metaheuristic algorithms commonly used for optimization, such as particle swarm optimization (PSO), genetic algorithms (GAs), and ant colony optimization (ACO). It is an efficient metaheuristic algorithm capable of identifying global optima with relatively low computational effort [31]. By employing it to study vibration mitigation, multi-parameter optimization of damping and stiffness properties can be investigated, which may offer a cost-effective means of designing customized seat dampers.

1.1 Research Gap and Novelty

Existing studies on bus seat vibration have largely focused on either experimental characterization or analytical modeling in isolation. EMT and FEA have been used separately to study seat dynamics [22-23], and rubber isolators have been explored in generic seat-suspension contexts [24]. There is limited published work that integrates full structural modal characterization of a real bus twin seat with experimentally grounded isolator selection and PSO-based parameter optimization. PSO was chosen for this problem because it can efficiently explore a multi-dimensional parameter space without relying on derivatives and can also handle the nonlinear, frequency-dependent characteristics of the seat–floor system. Moreover, prior PSO applications to seat vibration [31] have not been validated against measured seat FRF data from an actual in-service bus. This study's main goal is to demonstrate the combined EMT–FEA–PSO workflow as a repeatable engineering framework for WBV without structural modification. This is achieved by applying PSO to optimize isolator stiffness and damping based on a measured FRF baseline, evaluating three standard automotive rubber isolator types, and providing modal characterization of a real twin-seat bus frame using EMT and FEA. Specifically, the contribution lies in using PSO-based optimization to identify equivalent stiffness and damping parameters of the seat–floor system from experimentally measured FRF data, enabling vibration-reduction analysis at resonance frequencies.

2. Materials and Methods

In this section, EMT was conducted to characterize the seat's dynamic properties, while FEA was performed to assess the natural frequencies and the mode shape similarity with EMT. Vibration transmissibility tests were carried out both on board a bus and in a laboratory using a shaker as the excitation source. These tests introduced the metrics RMS, VDV, and SEAT values. Finally, PSO was employed to determine optimal damper parameters for minimizing vibration transmission.

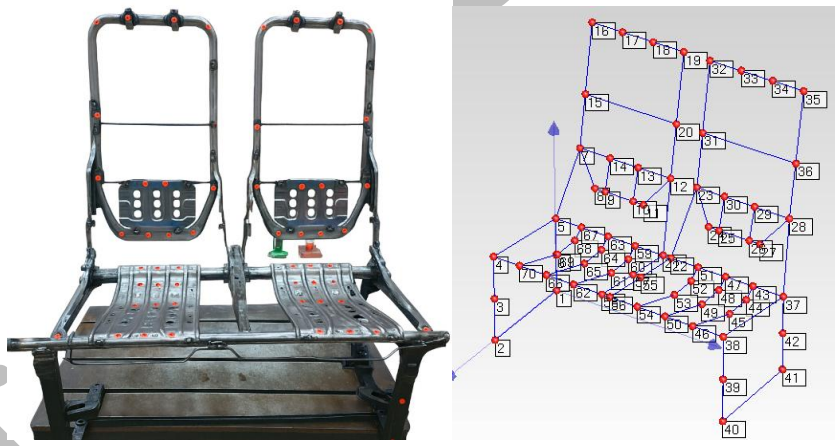

Figure 1. Bus seat frame and its MEScope Model

2.1 Experimental Modal Testing and FEA

Seventy measurement points were marked on the bus seat frame (Figure 1) as excitation locations. An impact hammer (PCB 086C03, 2.25 mV/N) was used to apply impacts, and responses were captured with a PCB triaxial accelerometer (100 mV/g) mounted on the frame using a magnet. FRFs were obtained using a roving impact technique with a fixed accelerometer location, and the data were processed via an NI 9234 data acquisition system and MEScope software. The seat frame was clamped to a steel base during testing. At the same time, every effort was made to replicate the fixed condition modeled in the FEA; however, in reality, some residual compliance at the clamping interface was unavoidable (in ANSYS, the mounting locations were represented using elastic support elements to capture the compliance observed during EMT). Each of the 70 marked points was impacted three times, and the responses were averaged to reduce signal noise. A finite element (FE) model of the seat frame was constructed in ANSYS Workbench for validation with the EMT results. The model was assigned as mild steel with Young's modulus E = 210 GPa, Poisson's ratio ν = 0.3. The model was assigned fixed supports at bolt locations. Modal analysis was performed on the model, and the natural frequencies and the mode shapes were simulated for comparison with the EMT data.

2.2 On-Board Vibration Data Collection

To obtain baseline vibration input data, measurements were conducted on a local public transport bus (Rapid Kuantan) operating along the Kuantan–Pekan state route (Figure 2). Accelerometers were mounted at two locations: one on the seat base leg adjacent to the floor, and the other on the seat surface, embedded in a 3D-printed seat pad that met ISO 2631-1 requirements. The triaxial accelerometer captured vibration in x, y, and z directions, which was used for RMS, VDV, and SEAT calculations in accordance with ISO 2631-1. Data were recorded using a laptop with DASYLab software and an NI 9432 module. RMS acceleration was used to quantify vibration levels because the signals were non-sinusoidal. In addition, SEAT values were calculated to assess the seat's isolation performance by comparing floor-to-seat vibration transmissibility [7]. Each measurement session comprised 180 seconds of continuous ride time, consistent with standard WBV assessment practice.

Figure 2. Vibration data collection on a bus

2.3 Laboratory Vibration Data Collection

For the transmissibility tests, measurements were done on an empty seat to obtain a consistent baseline. Adding a passenger mass would shift the resonance frequencies and dampen the response, but the primary goal here was to characterize the worst-case structural amplification of the seat itself. To accommodate the several types of rubber dampers used in this study, a custom bracket was designed and fabricated. A rigid metal frame was constructed to mimic the structural characteristics of a standard bus floor. To reproduce the low-frequency dynamic compliance of bus suspension and tires, four pneumatic air bellows were installed beneath the frame. Air bellows were selected because their stiffness and damping characteristics can be adjusted via inflation pressure, and they provide a broadband compliance at the base consistent with typical bus suspension natural frequencies (below 5 Hz). Although a full dynamic characterization of the bellows' stiffness was not performed, the primary role of the bellows in this study was to prevent rigid-body coupling between the frame and the laboratory floor, rather than to accurately replicate on-road suspension dynamics. An electrodynamic shaker was placed beneath the seat base frame to provide excitation across the 0–100 Hz range. Accelerometers (98.5 mV/g) were placed above and below each rubber damper, at the seat frame, and at the seat surface. Signals were acquired using an NI 9234 module and processed in MEScope and MATLAB.

(a) vibration transmissibility setup

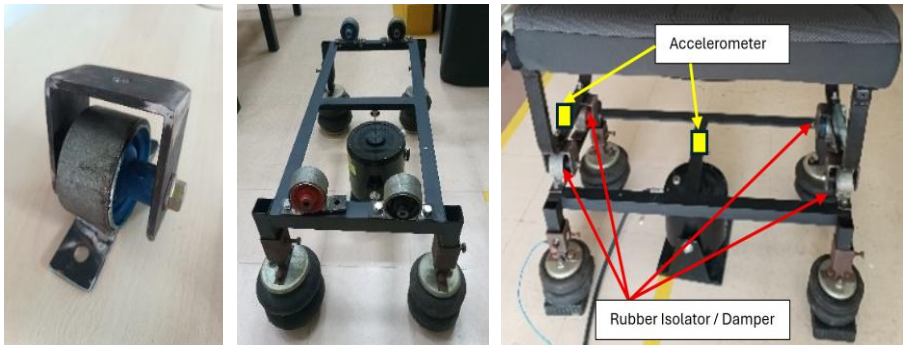

(b) rubber damper and its placement

Figure 3.

Vibration data were collected for: (i) baseline condition with the seat rigidly fixed to the base frame, and (ii) isolated condition with rubber dampers installed at all four seat legs (Figure 3a and 3b). SEAT values (Eq. 1) were computed to evaluate vibration isolation performance, using the frequency-weighted RMS acceleration at the seat surface (a_{seat}) relative to the base (a_{base}) [7]. A SEAT value < 90% indicates good vibration isolation, 90–110% indicates neutral performance, and > 110% indicates amplification. SEAT values were obtained both in on-road tests and in the laboratory for the seat with and without dampers.

$$SEAT = \left(\frac{a_{seat,RMS}}{a_{floor,RMS}}\right) x\ 100 \quad (1)$$

where a_{seat}RMS = frequency-weighted RMS acceleration measured on the seat surface and a_{floor}RMS = frequency-weighted RMS acceleration measured on the floor surface.

2.4 Data Analysis

In vibration and signal analysis, time-domain and frequency-domain representations are commonly used to detect how a signal varies over time and to display its amplitude as a function of frequency. Another representation is the Power Spectral Density (PSD), which quantifies how the signal's power is distributed across frequencies and provides a statistical perspective that is often useful for analyzing random vibrations. In essence, PSDs can be expressed as one-sided or two-sided. A two-sided PSD represents both positive and negative frequencies for mathematical completeness. In contrast, a one-sided PSD combines them into a single positive spectrum (which is more practical for real physical signals). Root-mean-square (RMS) is a metric that summarizes the overall signal energy into a single value and can be used to assess vibration severity. Another metric used in the experiment is Vibration Dose Value (VDV), which emphasizes transient shocks and also serves as a representation of realistic human WBV exposure.

3. Results and Discussion

In this section, EMT results are reported to identify the natural frequencies and mode shapes of the bus seat, followed by FEA validation. On-board vibration measurement data will be used to calculate transmissibility, yielding the RMS, VDV, and SEAT metrics. These metrics will be correlated to the simulated laboratory measurements to quantify the effectiveness of rubber dampers in reducing vibration. Finally, the PSO study will be presented, which highlights the optimal damper parameters for improved vibration isolation and passenger comfort.

3.1 Experimental Modal Analysis

The EMT results revealed six vibration modes of the bus seat structure in the range of 0-100 Hz. The first mode appeared at 28 Hz, corresponding to in-phase forward–backward bending of the seat back. This mode is consistent with the backrest geometry, allowing flexibility in the fore–aft direction. The second mode was lateral bending at 38 Hz, with the left and right sides of the backrest moving in opposite directions. The third mode, at 62 Hz, represents fore–and–aft bending but is out of phase between the twin seats. The fourth mode is at 69 Hz with lateral bending motion and in-phase between the twin seats. The fifth mode was identified at 78 Hz, representing second-order fore–aft bending. The final mode in the range was a twisting mode at 95 Hz around the seatback vertical axis. In summary, modes 1 and 2 were the most significant, as they exhibited the largest amplitude responses. These modes may coincide with the frequencies excited by road inputs (broadband), so resonance at these points could amplify vibration felt by passengers. FRF plots confirmed the presence of high amplification and limited damping near the first two bending modes.

3.2 Experimental Modal Analysis

The FEA model done in ANSYS shows the mode shapes and the natural frequencies of the twin seat, which are comparable to the experimental findings after modifications. An iterative simulation was performed by varying the elastic support stiffness and mesh density (from fine to coarse) to achieve natural frequencies that were comparable between the FEA model and the EMT data. The fundamental mode at 28 Hz, characterized by in-phase fore–aft bending, correlates to the mode found in the EMT. Similar mode-matching was performed for the other five modes. Table 1 shows that the average frequency difference between EMT and FEA results is approximately 10–15% across all modes. This 10–15% frequency deviation is considered acceptable given the geometric simplifications required to model the seat frame in ANSYS. In ANSYS, elastic support elements were introduced at the mounting locations to account for the actual experimental boundary inaccuracy under the fixed condition (Figure 4). To account for the observed boundary compliance, the FEA stiffness values were adjusted to a range of 1×10^5 to 5×10^6 N/m. In the EMT, the seat was clamped to a steel table, but that does not perfectly replicate a fully fixed support, as some compliance existed at the clamping interface. The mode shapes for the first two modes are illustrated in Figures 4a and 4b.

The overall results indicate that the decision to introduce isolators at the seat legs can be effective if they filter vibration amplitudes at the floor, reducing excitation of the seat resonance frequencies, and the damper will also damp out the resonance peaks.

Table 1. Mode shapes and corresponding natural frequency

Mode	Description	EMT	FEA
1	Seatback bending (fore-aft, in-phase)	28 Hz	32 Hz
2	Lateral bending (out-of-phase)	38 Hz	43 Hz
3	Fore-aft bending (out-of-phase)	62 Hz	68 Hz
4	Lateral bending (in-phase)	69 Hz	75 Hz
5	Second-order fore-aft bending	78 Hz	85 Hz
6	Seatback torsion (twisting)	95 Hz	110 Hz

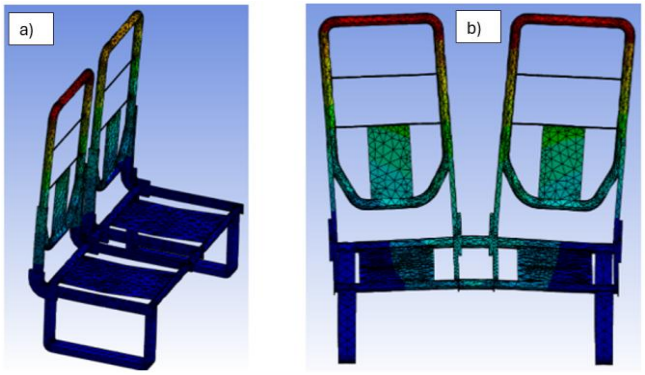

Figure 4. (a) FEA mode shape at 32 Hz, (b) FEA mode shape at 43 Hz

3.3 On-board Measurements

Vibration measurements were carried out on the Kuantan–Pekan route at bus speeds ranging from 30 to 80 km/h. Data were collected at 10 km/h intervals, with the longest recording (180 s) obtained at 70–80 km/h, corresponding to the bus's typical cruising speed on interstate roads. Accelerometers were positioned at the seat base (floor level) and at the seat surface to capture input and transmitted vibrations, respectively. An example of vibration data with RMS collected at 60 km/h is shown in Figure 5.

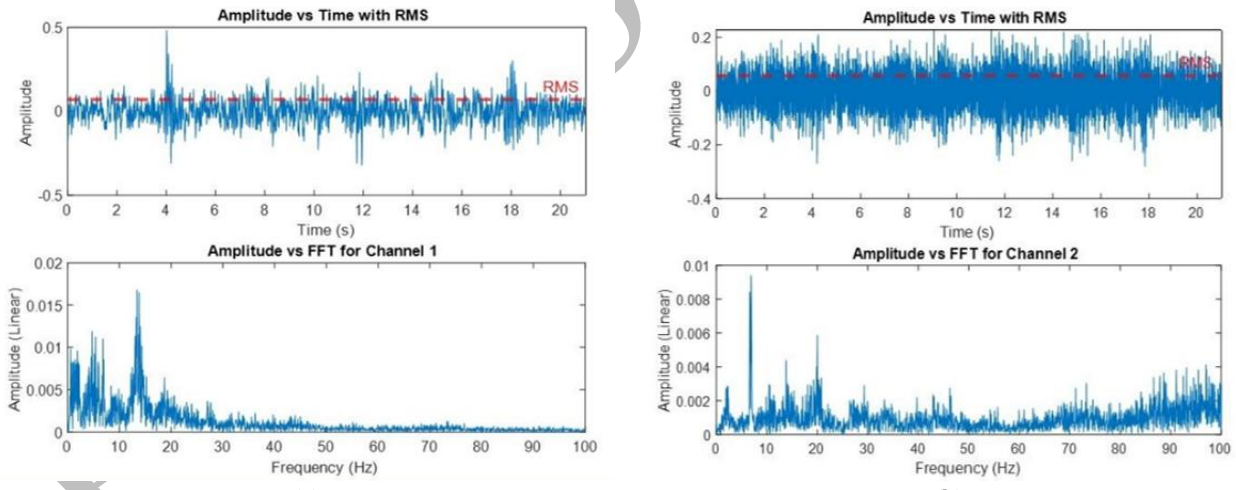

(a) (b)

Figure 5. Vibration data from (a) bus seat floor, (b) vibration data from seat cushion (right) at 60 km/h

Table 2 summarizes the RMS acceleration and VDV for all the tested bus speeds. VDV of the system is given by:

$$VDV = \left(\int_0^T a_w\,(t)^4\,dt\right)^{\frac{1}{4}} \tag{2}$$

where $a_w\,(t)$ is frequency weighted acceleration as a function of time (in m/s²) [using weighting filters from ISO 2631-1, t is the duration of measurement (in seconds), and ∫ is the integration over time.

Table 2 shows that the RMS of both the seat and the floor increases as the bus speed increases from 30 to 80 km/h. The increase is more notable between 30 and 40 km/h, while more gradual towards 60 km/h. At 70–80 km/h, the vibration amplitude rises more drastically. For the VDV metric, a significant jump at higher speeds is observed, reaching 1.611 $m/s^{1.75}$ at the seat surface during 70–80 km/h bus speed. It is known that prolonged exposure to vibration can increase the risk of discomfort and health effects, in line with WBV guidelines. According to ISO 2631, a certain level of transmissibility poses a health risk if exposure is frequent or prolonged. The Standard specifies health-based frequency

weighting for WBV assessment in the frequency range of 0.5 to 80 Hz. However, in our measurement, we focused on the 20–100 Hz range specifically for structural characterization and isolator design. This frequency range encompasses all identified structural resonances of the seat frame.

Table 2. RMS and VDV values at different bus speeds

Bus Speed (km/h)	RMS (m/s^2)		VDV ($m/s^{1.75}$)		SEAT (%)
	Seat	Floor	Seat	Floor	
30	0.0344	0.0242	0.1088	0.0767	142
40	0.0660	0.0320	0.2087	0.1013	206
50	0.0553	0.0461	0.1750	0.1458	120
60	0.0658	0.0546	0.2080	0.1725	121
70-80 (180 secs)	0.1040	0.0601	1.6108	0.9307	173

The results indicate that the seat tends to amplify vibration, with seat-level RMS values consistently exceeding those at the floor. It can be deduced from the on-board measurements that vibration exposure increases with vehicle speed, with the worst levels occurring at 70–80 km/h (cruising speed). A similar deduction can be made using the SEAT metric, which identifies how effectively the seat isolates vibration from the floor to the passenger. A SEAT value below 100% indicates attenuation, whereas values above 100% indicate amplification. The results clearly show that the bus seat amplifies vibration across all speeds, with SEAT values consistently exceeding 100%. For the SEAT metric in Table 2, the highest amplification occurs at 40 km/h (> 200%). At highway speeds (70–80 km/h), the SEAT is high (173%), which confirms that the absence of an isolator between the seat and floor leads to vibration transmission and amplification. In other words, a bus seat, while being rigidly bolted to the floor, does not provide effective vibration isolation and can, in fact, worsen passenger exposure.

3.4 Damper Evaluation

To investigate possible improvements, three different types of rubber dampers were tested as isolators between the seat and the floor in a laboratory setup. It is noted that effective vibration isolation can be achieved either by reducing the mounting stiffness (which lowers the natural frequency of the seat system below the excitation range) or by adding damping (which attenuates resonance amplitudes). The introduction of rubber isolators or dampers reduces vibration transmission from the floor to the seat at frequencies above the system's natural frequency. Although the compliant support introduces low-frequency rigid-body motion, it occurs in a range where human sensitivity is lower. Additionally, inherent material damping limits resonance amplification. As a result, the overall vibration experienced by the passenger is reduced, improving ride comfort.

In this study, rubber bushing dampers were selected mainly because they are easy and practical to install under a bus seat and have specific stiffness that can be modified by altering shape and size. The goal of using this damper (also known as a roll mount or bushing) is to reduce the stiffness coupling between the floor and the seat structure, thereby suppressing the resonance peaks. This dual role is consistent with the later observation in Figure 10, where peak reductions occur at the resonance frequencies. Each damper was evaluated for its ability to isolate vibration based on SEAT measurements, as shown in Figure 6 and Table 3.

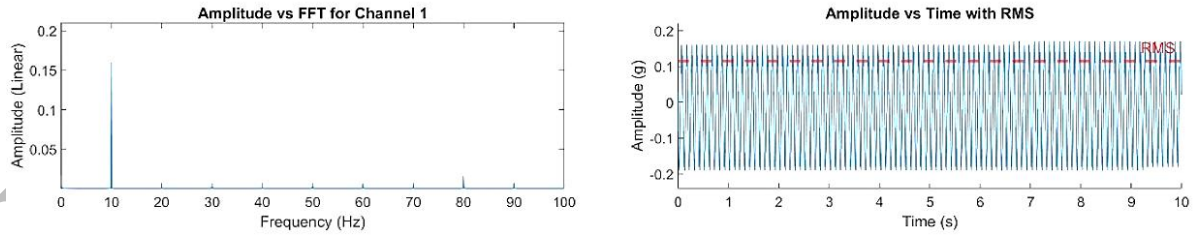

Figure 6. Example FFT and time waveform of each damper (at 10 Hz sinusoidal excitation)

Table 3 shows that Damper 1 provided the best isolation, reducing the RMS acceleration by approximately 33%. Damper 2 exhibited almost identical values above and below (0.24), suggesting it is too stiff to absorb vibration effectively. Damper 3 slightly amplified vibration, with higher RMS above the damper (0.10), which could worsen WBV exposure if implemented. Overall, the results demonstrate that damper selection plays a noticeable role in seat vibration isolation. Among the tested damper samples, Damper 1 shows potential to isolate the bus seat from the floor, while the others are ineffective.

Table 3. Damper and respective RMS values

	Amplitude (Above)	Amplitude (Below)	RMS (Above)	(RMS) (Below)	SEAT (%)
Damper 1	0.14	0.16	0.10	0.15	67
Damper 2	0.24	0.24	0.17	0.17	100
Damper 3	0.10	0.09	0.07	0.06	116

3.5 Rubber Damper Material Characterization

The tensile tests on the three rubber damper samples (20.8 cm × 1.25 cm × 3.4 cm) showed consistent elastic behavior typical of standard rubber stiffness. The Young's modulus E was obtained from the initial linear region of the stress–strain curve. Stress was calculated as the applied force divided by the original cross-sectional area, and strain as the elongation divided by the initial gauge length. From the linear regions of the curves (Figure 8), the calculated modulus values ranged between 0.32 MPa and 0.34 MPa, as listed in Table 4. Minor differences between samples are thought to be caused by small variations in specimen cut size and clamping alignment or force.

The modulus value can be used to improve the finite element model, resulting in more accurate mode shapes and natural frequencies. In addition, accurate measurement of the rubber's Young's modulus is important for the later PSO optimization. This allows the PSO algorithm to search for the best stiffness and damping settings based on actual material properties rather than assumed values, thereby making the vibration control design more reliable. In the PSO, the stiffness $k = EA/L$ defines how much the rubber layer resists deformation under load, influencing both seat transmissibility and vibration isolation efficiency. The goal is for the PSO to search for the most reliable combination of stiffness and damping ratio that minimizes vibration from the bus floor to the seat.

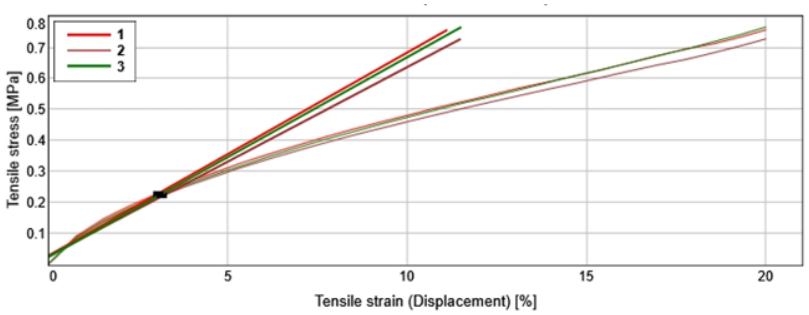

Figure 8. Stress-strain curve of the rubber damper (3 samples)

Table 4. Young's modulus of the rubber samples

Specimen	Force at Tensile Strength (F) [kN]	Displacement at Break $\boldsymbol{\Delta L}$ [mm]	Gauge Length $\boldsymbol{L_0}$ [mm]	Cross-Sectional Area $\boldsymbol{A_0}$ [mm²]	Young's Modulus $\boldsymbol{E = \frac{FL_0}{A_0 \Delta L}}$ [MPa]
Sample 1	6.55	0.76	23	425	0.33
Sample 2	6.09	0.73	23	425	0.32
Sample 3	6.44	0.77	23	425	0.34

3.6 Rubber Damper Material Characterization

In this study, PSO is employed to determine the optimal stiffness (k_r) and damping (c_r) of rubber isolators placed under the four legs of a bus seat. PSO is particularly suitable for this problem because it efficiently searches the multi-dimensional parameter space without requiring derivative information. It can also handle the seat-floor system's nonlinear, frequency-dependent behavior.

In the PSO model, several assumptions are made to simplify the simulation such that human biodynamic effects are not modeled (the occupant is represented as a lumped mass), where the focus is always to measure the effectiveness of vibration isolation of the damper itself before reaching the seat, and not to study the human body's many DOF responses. In addition, the base excitation is approximated as a white-noise spectrum rather than a measured road profile due to the complexity of powering the shaker with actual road input. These simplifications are acknowledged as limitations but are not considered restrictive to determining the effectiveness of the isolator itself. Henceforth, the PSO results should be interpreted primarily as design guidance for isolator parameter selection rather than as precise predictive performance data under real operating conditions.

The seat and occupant system (total mass of 100 kg is modeled as a single lumped mass (1-DOF system), while the bus floor is represented using a base excitation model with equivalent mass, damping, and stiffness. This simplification is adopted to focus on predicting the vibration response amplitude transmitted to the seat and seated occupant, rather than capturing detailed multi-body interactions within the human–seat system. The excitation is modeled as a broadband random vibration representing road-induced disturbances in the 20–100 Hz range, which coincides with the dominant seat structural resonance frequencies identified from the EMT.

3.6.1 Objective Function

In the study of bus seat vibration isolation, the seat is typically modeled as a two-degree-of-freedom system comprising the seat itself and the supporting floor or chassis. The main objective is to minimize seat displacement variance under dynamic excitation that can impact occupant comfort and safety. To achieve this, an objective function representing the vibration response is defined and used within optimization algorithms such as PSO. A closed-form analytical function derived from the 2-DOF will be used as the objective function. The objective function in this study is the total variance of the seat displacement, $\sigma_{x_s}^2$, which quantifies the overall vibrational energy transmitted to the occupant through the seat.

It is computed from the seat displacement power spectral density (PSD), $S_{x_s}(\omega)$, by integrating over the frequency range of interest:

$$\sigma_{x_s}^2 = \int_0^{\omega_{\max}} S_{x_s}(\omega)\, d\omega \tag{3}$$

where ω is the angular frequency (rad/s), and $\omega_{\max}$ corresponds to the highest frequency considered in the analysis. The seat displacement PSD is obtained by multiplying the squared magnitude of the transfer function from base acceleration to seat displacement, $|H(\omega)|^2$, by the base acceleration PSD, $S_a(\omega)$:

$$S_{x_s}(\omega) = |H(\omega)|^2\ S_a(\omega) \tag{4}$$

The transfer function $H(\omega)$ is derived from a linear two-degree-of-freedom (2-DOF) model of the seat-floor system, which includes the seat mass m_s, floor patch mass m_b, seat isolator stiffness k_s, and damping c_s, and suspension stiffness k_{susp} and damping c_{susp}. The system equations in the frequency domain can be expressed in matrix form as:

$$\underbrace{\begin{bmatrix} -k_s - i\omega c_s + m\omega^2 & k_s + i\omega c_s \\ k_s + i\omega c_s & -(k_s + k_{usp}) - i\omega(c_s + c_{usp}) + m_b\omega^2 \end{bmatrix}}_{A(\omega)} \begin{bmatrix} X_s(\omega) \\ X_b(\omega) \end{bmatrix} = \begin{bmatrix} 0 \\ m_b(-\omega^2 X_g(\omega)) \end{bmatrix} \tag{5}$$

Here, $X_s(\omega)$and $X_b(\omega)$are the seat and floor displacements in the frequency domain, and $X_g(\omega)$is the base displacement due to the road or vehicle excitation. The right-hand-side vector represents the forcing due to the base acceleration, which acts directly on the floor mass and indirectly excites the seat. Solving for $X_s(\omega)$gives the transfer function from base acceleration to seat displacement:

$$H(\omega) = \frac{X_s(\omega)}{X_g(\omega)} = \frac{\text{cofactor of } A_{12} \text{ corresponding to } X_s}{\det(A(\omega))} \tag{6}$$

This transfer function allows computation of the seat PSD and, subsequently, the total variance $\sigma_{x_s}^2$, which serves as the objective function for reducing the vibration amplitude. Therefore, the objective function for PSO can be formulated as:

$$f(k_s, c_s) = \sigma_{x_s}^2 = 2\int_0^{\omega_{\max}} |H(\omega)|^2\ S_a(\omega)\, d\omega \tag{7}$$

In Eq. 7, the factor of 2 shows up because the PSD is defined as two-sided per rad/s. Therefore, the total variance includes both positive and negative frequencies. The base acceleration PSD, $S_a(\omega)$, represents the spectral distribution of the floor vibration energy or the system input. Usually, in numerical simulations, the base acceleration PSD, $S_a(\omega)$, is modeled as a white spectrum with a constant amplitude, for example $S_0 = 1 \times 10^{-6}\ \text{m}^2/\text{s}^3/\text{rad}$ which represents broadband random excitation.

Minimizing $\sigma_{x_s}^2$ directly reduces overall seat vibration energy across all frequencies, particularly in the dominant low-frequency range near resonance, making it a meaningful metric for minimizing seat vibration. The optimizer searches for the combination of seat damper stiffness and damping that minimizes the total variance, thereby attenuating resonant peaks in the frequency range that dominates the occupant's vibrational exposure. By focusing on the variance rather than individual peak amplitudes, the method balances the trade-offs between low-frequency isolation and high-frequency transmission.

Figure 9(a) plots the seat displacement variance (σ_{xt}^2) as a function of frequency, both before and after PSO-based optimization of the seat and floor damping. The dashed red curve represents the initial system with nominal damping values, while the solid blue curve shows the system after optimization. From the plot, it can be seen that the resonance peaks around the seat's natural frequency have been reduced after optimization. The peak amplitudes are lower, indicating improved vibration isolation and reduced seat motion at critical frequencies. Figure 9(b) presents a 3D surface of peak seat displacement variance (σ_{xt}^2) vs. the isolator stiffness (k_r) and damping (c_r). The vertical axis represents the peak variance, while the horizontal axis shows the range of rubber stiffness and damping. The surface plot indicates that lower peak variance can be achieved over a wide region of stiffness and damping combinations. This shows that multiple combinations of rubber properties can provide effective vibration isolation. This, in turn, will give better flexibility in material selection and design. The plot shows that an increase in stiffness can be compensated by a decrease in damping, and vice versa, yielding similar peak reductions. This visualization will allow designers to choose rubber properties based on practical constraints such as size, cost, or comfort while still ensuring reduced seat vibrations.

The earlier plot shows the relationship between stiffness and damping and their influence on the overall vibration variance using an analytical model. Then, baseline data (a case without a rubber layer) were obtained from the measured FRF of the seat–floor system. The PSO algorithm was then applied directly to the experimental data to search for optimal stiffness and damping parameters that minimize vibration amplitudes across the critical resonance frequencies identified during testing. The resulting plot in Figure 10 compares the measured FRF with the simulated (after-PSO) response, illustrating the effect of introducing optimized rubber mount properties in attenuating resonance peaks and improving ride comfort. The PSO-based procedure in this study is used as a parameter identification and curve-fitting approach to determine equivalent stiffness and damping values that best represent the observed FRF trend. The resulting 'after-PSO FRF' therefore reflects an optimized fitted response rather than a full physics-based simulation of a modified structural

system. This approach is used to quantify the effective dynamic properties that minimize vibration response within the identified resonance frequency range.

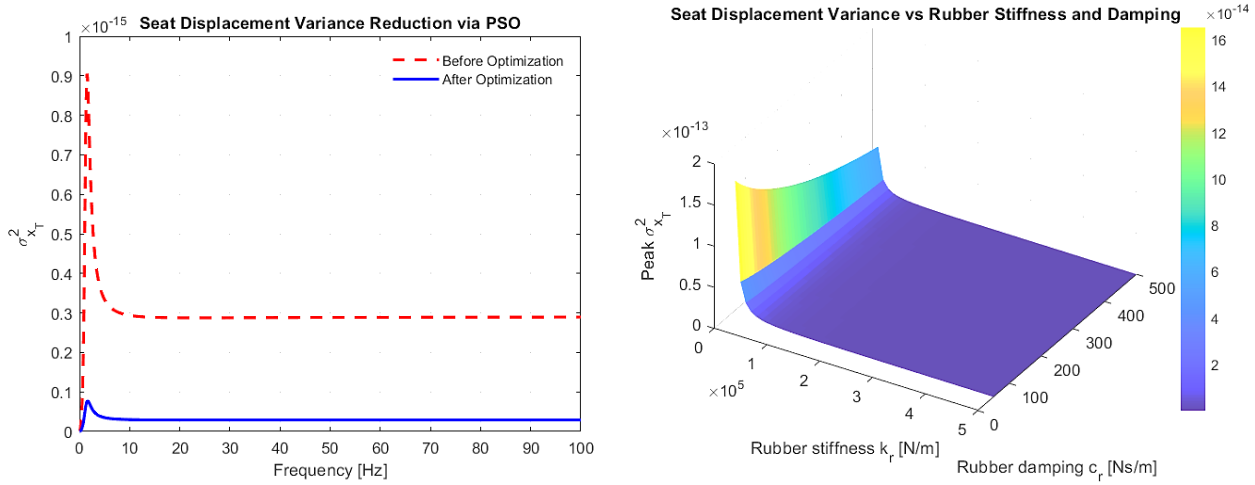

(a) (b)

Figure 9. Seat displacement (a) variance (σ_{xt}^2) vs (b) frequency

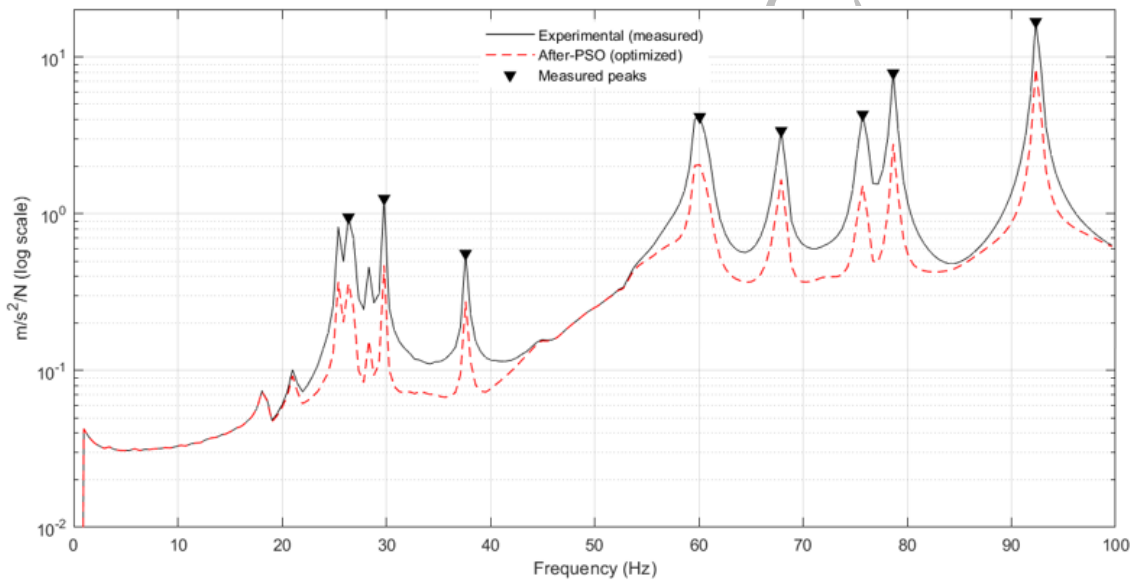

Figure 10. FRF response on the seat from experimental and PSO

For Figure 10, the PSO search was conducted within realistic bounds of $k_s = [5 \times 10^4, 8 \times 10^5]$ N/m and $c_s = [20, 3000]$ Ns/m, with nominal values $k_{\text{ref}} = 3 \times 10^5$ N/m and $c_{\text{ref}} = 200$ Ns/m. Control parameters $\gamma_c = 1.0$, $\gamma_k = 0.01$, and max_attenuation $= 0.5$ were used to regulate damping and stiffness influence on resonance peak reduction. Figure 10 shows the experimental (measured) and the After-PSO (optimized) condition of the seat response. The experimental curve shows the frequency response of the bus seat without a damping isolator. It serves as the baseline behavior, capturing the seat's actual vibrations and resonance peaks. Peaks in this curve correspond to the system's modal frequencies, points at which the seat naturally amplifies vibrations in response to excitations. These are the frequencies that the optimization aims to mitigate.

The After-PSO curve represents the FRF after optimizing the rubber stiffness and damping using PSO. The optimization is designed to attenuate the measured peaks by applying a Gaussian-shaped reduction around each modal frequency, thereby effectively reducing the amplitude at resonance. This demonstrates how adjusting the seat's leg-rubber isolator can reduce peak vibration amplitude, improving ride and comfort. The PSO-optimized results are based on numerical parameter identification using the measured baseline FRF and have not been experimentally validated with modified rubber isolator configurations. As such, the presented results should be interpreted as a model-based estimation of potential vibration reduction rather than a fully validated physical implementation.

A parametric study was subsequently conducted to understand further how variations in seat isolator properties influence the overall vibration response. The frequency- and time-domain representations of the data may not fully capture the overall vibration energy transmitted to the seat across a broader frequency band. Therefore, a surface plot was

generated to show the seat's RMS acceleration response over the 20–80 Hz range as a function of stiffness (k_s) and damping (c_s). This analysis illustrates the vibration severity of different damper combinations and their effect on comfort and dynamic isolation.

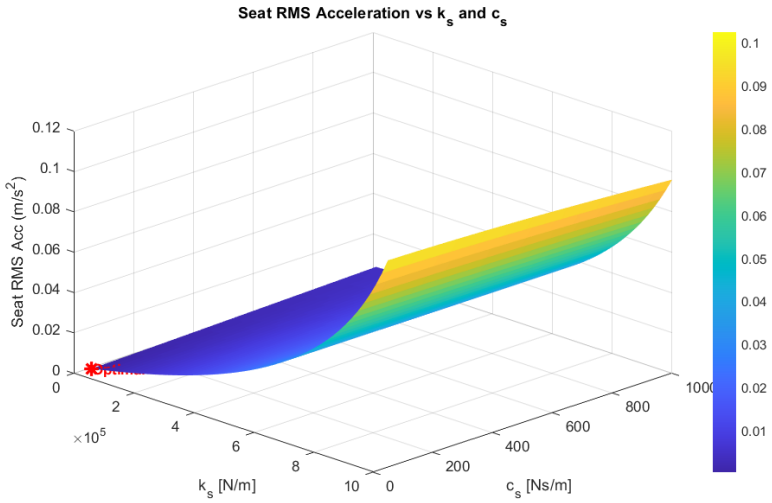

Figure 11. Seat RMS acceleration vs seat stiffness (k_s) and damping (c_s)

The surface plot of seat RMS acceleration as a function of seat stiffness (k_s) and damping (c_s) (Figure 11) reveals the sensitivity of seat vibration to isolator properties in the 20–80 Hz frequency range. The plot shows a clear valley in the low k_s region, indicating that softer seat stiffness can significantly reduce seat acceleration. This vibration isolation works better by improving vibration at higher frequencies. Furthermore, along the low-stiffness valley, the RMS acceleration varies moderately with damping, suggesting that moderate damping values are sufficient to control resonance peaks without substantially affecting high-frequency isolation. At very high damping, it can slightly increase the RMS acceleration due to overdamping effects.

In practice, minimizing k_s (using a softer damper in the seat legs) allows the seat to "float" more by decoupling from floor vibrations. Damping (c_s) represents the energy dissipation of these mounts, which helps control resonances by reducing resonance amplitude. In summary, Figure 11 demonstrates that reducing seat stiffness is the primary factor for minimizing acceleration, while damping provides finer tuning in the optimal low-stiffness region. The red star on the plot identifies the optimal parameters determined by the PSO process, corresponding to the stiffness-damping combination that minimizes the seat RMS acceleration.

4. Conclusions

The vibration behavior of a bus seat was examined using experimental, numerical, and optimization methods. EMT was used to characterize and validate the seat dynamics through FEA, confirming that the seat structure exhibits six vibration modes in the 20–100 Hz range that can amplify floor-level vibration input. On-road measurements showed that vibration magnitude (RMS) and severity (VDV) rise with bus speed, while SEAT values above 100% confirmed that the seat without isolators amplifies vibration transmitted to passengers. Laboratory testing of three rubber damper types revealed that the best-performing damper achieved a SEAT of 67%, demonstrating its potential to reduce vibration.

PSO optimization was used to identify the most effective stiffness and damping parameters to attenuate resonance peaks and minimize seat RMS acceleration across the frequency range. PSO results provide design guidance under idealized modeling assumptions; validation can be performed through physical prototype testing using the optimized isolator parameters. The findings demonstrate that correctly selected rubber isolators can improve seat vibration isolation and passenger ride comfort. The combined EMT–FEA–PSO methodology offers a practical framework for improving WBV in public transport seating systems and can be extended to other vehicle or machinery support structures.

Acknowledgements

The authors acknowledge the support provided by Universiti Malaysia Pahang Al-Sultan Abdullah for research facilities and equipment access for this investigation.

Funding

Universiti Malaysia Pahang, Al-Sultan Abdullah, PGRS230388 (Postgraduate Research Grant), partially supported this study.

Declaration of Competing Interest

The author declares no conflicts of interest.

CRediT Authorship Contribution Statement
Z. Mohamed (Conceptualisation; Methodology; Validation; Resources; Writing; Supervision)
S.M. Tasnim Mahbub (Experimental testing; Data curation; Investigation)
R. Khairuddin (Data curation; Writing - editing)

Availability of Data and Materials
The data supporting this study's findings are available on request from the corresponding author.

Ethics Statement
This study did not involve human participants or animals. Ethical approval was therefore not required.

Generative Artificial Intelligence Declarations
The authors claim that artificially intelligent-assisted technologies, such as generative AI, were not used to generate content, ideas, or theories. We have just utilized AI to enhance readability and refine the language. This was used with extreme human control and oversight. The authors take full responsibility for reviewing and approving the content.

References

[1] M. Moore, Y. Yao, A. Seifi, S. Rakheja, R. Sedaghati, "Effects of non-neutral head-neck posture on seat-to-head vibration transmissibility response characteristics in rotorcraft pilot/crew," *International Journal of Industrial Ergonomics*, vol. 113, 2026. https://doi.org/10.1016/j.ergon.2026.103928

[2] W. Ding, L. Wang, Z. Chen, H. Ao, H. Yan, Z. Li, "Influence of seat-human contact on discomfort caused by vertical whole-body vibration under Class C road excitation," *International Journal of Industrial Ergonomics*, vol. 110, 2025. https://doi.org/10.1016/j.ergon.2025.103816

[3] F. Tajdari, C. Messiou, R. Happee, G. Papaioannou, "Can seat suspensions mitigate motion sickness and enhance vibration comfort while being driven? A subjective assessment of the K-Seat," *Applied Ergonomics*, vol. 135, 2026. https://doi.org/10.1016/j.apergo.2026.104772

[4] E. Davies, F. Nasiri, "A comparative vibroacoustic performance and comfort assessment of conventional and electric buses: The city of Montreal case study," *Transportation Research Procedia*, vol. 44, 2026. https://doi.org/10.1016/j.tbs.2026.101244

[5] X. Ma, Y. Li, J. Zhang, "A biomechanics-informed nonlinear dynamic model for seated occupant exposed to vertical vibration and impact," *Mechanical Systems and Signal Processing*, vol. 254, 2026. https://doi.org/10.1016/j.ymssp.2026.114410

[6] A. König, C.-J. Kat, N. Keough, H. M. Oberholzer, J. Myburgh, "Effects of seated whole-body vibration on the lumbar spine: A Sprague-Dawley animal model," *Journal of Biomechanics*, vol. 201, 2026. https://doi.org/10.1016/j.jbiomech.2026.113261

[7] P. Grabski, D. Frej, M. Jaśkiewicz, L. Karwala, R. Chaba, "Experimental analysis of vertical vibrations in child car seats with a swivel base," *Transportation Research Procedia*, vol. 93, pp. 236–241, 2026. https://doi.org/10.1016/j.trpro.2025.11.036

[8] V. F. M. Remy, B. Antoine, I. G. Canu, "The bus-ergonomics matrix for comprehensive evaluation of buses and bus drivers' exposure," *Applied Ergonomics*, vol. 128, 2025. https://doi.org/10.1016/j.apergo.2025.104550

[9] A. Said, M. Kwikima, A. Ripanda, "Ergonomic challenges and health implications for long-distance bus passengers in Tanzania," *Advanced Design Research*, vol. 3, no. 2, pp. 159–170, 2025. https://doi.org/10.1016/j.ijadr.2026.03.002

[10] R. P. Blood, M. A. Johnson, P. W. Wasserman, "Whole-body vibration exposures in metropolitan bus drivers," *Journal of Sound and Vibration*, vol. 329, no. 1, pp. 109–120, 2010. 10.1016/j.jsv.2009.08.030

[11] O. Thamsuwan, P. W. Wasserman, N. Miyashita, "Whole-body vibration exposures in bus drivers: A field study," *International Journal of Industrial Ergonomics*, vol. 43, no. 5, pp. 495–502, 2013. https://doi.org/10.1016/j.ergon.2012.10.003

[12] M. Bovenzi, "Low back pain disorders and exposure to whole-body vibration in professional drivers," *International Journal of Industrial Ergonomics*, vol. 17, no. 5, pp. 367–377, 1996. https://doi.org/10.1016/S0146-0005(96)80056-5

[13] D. Sekulić, S. Rusov, V. Dedović, S. Šalinić, D. Mladenović, and I. Ivković, "Analysis of bus users' vibration exposure time," *International Journal of Industrial Ergonomics*, vol. 65, pp. 26–35, 2018. https://doi.org/10.1016/j.ergon.2018.01.017

[14] D. Sekulić, V. Dedović, S. Rusov, S. Šalinić, A. Obradović, "Analysis of vibration effects on the comfort of intercity bus users by oscillatory model with ten degrees of freedom," *Applied Mathematical Modelling*, vol. 37, no. 18–19, pp. 8629–8644, 2013. https://doi.org/10.1016/j.apm.2013.03.060

[15] G. Coquel, C. Fillol, "Analysis of ground-borne noise and vibration levels generated by buses," *Procedia Engineering*, vol. 199, pp. 2699–2704, 2017. https://doi.org/10.1016/j.proeng.2017.09.564

[16] M. Z. Nuawi, A. R. Ismail, M. J. M. Nor, M. M. Rahman, "Comparative study of whole-body vibration exposure between train and car passengers: A case study in Malaysia," *International Journal of Automotive and Mechanical Engineering*, vol. 4, pp. 490–503, 2011. https://doi.org/10.15282/ijame.4.2011.10.0040

[17] International Organization for Standardization, "Mechanical vibration and shock – Evaluation of human exposure to whole-body vibration – Part 1: General requirements," 1997.
[18] J. L. Van Niekerk, R. S. Pielemeier, M. J. Greenberg, "The use of SEAT values to predict seat transmissibility," *Journal of Sound and Vibration*, vol. 260, no. 5, pp. 867–888, 2003. https://doi.org/10.1016/S0022-460X(02)00934-3
[19] J. H. Varterasian, R. R. Thompson, "Human response to whole-body vibration: Transmissibility and subjective discomfort," *Human Factors*, vol. 19, no. 6, pp. 683–693, 1977. https://doi.org/10.1006/jsvi.2002.5498
[20] M. H. U. Bhuiyan, Y. Matsumoto, M. J. Griffin, "Effects of whole-body vibration on driver drowsiness," *Journal of Sound and Vibration*, vol. 519, p. 117540, 2022. https://doi.org/10.1016/j.jsr.2022.02.009
[21] S. A. Adam, N. A. A. Jalil, K. A. M. Razali, Y. G. Ng, M. F. Aladdin, "Mathematical model of suspension seat-person exposed to vertical vibration for off-road vehicles," *International Journal of Automotive and Mechanical Engineering*, vol. 16, no. 2, pp. 6773–6782, 2019. https://doi.org/10.15282/ijame.16.2.2019.22.0509
[22] R. Rahmani, M. Mahdavi, A. Shafei, "Modal testing and vibration characterization of vehicle seats for ride comfort evaluation," *Mechanical Systems and Signal Processing*, vol. 120, pp. 36–48, 2019. https://doi.org/10.1177/0954406219858172
[23] K. Chen, X. Liu, Y. Yang, "Ride comfort analysis and hierarchical parameter identification using multi-objective optimization," *Mechanical Systems and Signal Processing*, vol. 138, p. 106556, 2020. https://doi.org/10.1016/j.measurement.2020.108142
[24] S. Kumar, B. Ramesh, "Optimization of seat suspension parameters for ride comfort," *Applied Acoustics*, vol. 164, p. 107242, 2020. https://doi.org/10.1007/s40032-014-0156-7
[25] M. Al-Dhahebi, A. K. Junoh, Z. Mohamed, W. Z. A. W. Muhamad, "A computational approach for optimizing vehicles' interior noise and vibration," *International Journal of Automotive and Mechanical Engineering*, vol. 14, no. 4, pp. 4690–4703, 2022. https://doi.org/10.15282/ijame.14.4.2017.8.0369
[26] O. Zargar, A. Masoumi, A. O. Moghaddam, "Investigation and optimization for the dynamical behaviour of the vehicle structure," *International Journal of Automotive and Mechanical Engineering*, vol. 14, no. 2, pp. 4196–4210, 2022. https://doi.org/10.15282/ijame.14.2.2017.7.0336
[27] A. Jamali, M. H. Hassan, L. Roslan, M. S. Hadi, "Implementation of evolutionary algorithms to parametric identification of gradient flexible plate structure," *International Journal of Automotive and Mechanical Engineering*, vol. 20, no. 3, pp. 10559–10573, 2023. https://doi.org/10.15282/ijame.20.3.2023.01.0815
[28] R. Rosli, Z. Mohamed, G. Priyandoko, "Semi active s eat suspension system using modified intelligent active force control," *International Journal of Automotive and Mechanical Engineering*, vol. 18, no. 1, pp. 8498–8504, 2021. https://doi.org/10.15282/ijame.18.1.2021.09.0644
[29] N. Nawayseh, "A mathematical model of the apparent mass of the human body under fore-and-aft whole-body vibration," *International Journal of Automotive and Mechanical Engineering*, vol. 13, no. 3, pp. 3613–3627, 2022. https://doi.org/10.15282/ijame.13.3.2016.7.0297
[30] C. W. Shan, M. I. Ghazali, M. I. Idris, "Improved vibration characteristics of flexible polyurethane foam via composite formation," *International Journal of Automotive and Mechanical Engineering*, vol. 7, pp. 1031–1042, 2022. https://doi.org/10.15282/ijame.7.2012.19.0084
[31] G. Papaioannou, C. Papadimitriou, S. Pnevmatikos, "A hybrid particle swarm optimization approach for vehicle suspension design," *Journal of Sound and Vibration*, vol. 442, pp. 242–258, 2019. https://doi.org/10.1016/j.engappai.2010.02.002